Tuning the Electronic Properties of Single-Atom Pt Catalysts by Functionalization of the Carbon Support Material

Mehdi Mahmoodinia,[†] Per-Olof Åstrand,[*,†] and De Chen[‡]

†Department of Chemistry, Norwegian University of Science and Technology (NTNU),
N-7491 Trondheim, Norway
‡Department of Chemical Engineering, Norwegian University of Science and Technology
(NTNU), N-7491 Trondheim, Norway

E-mail: per-olof.aastrand@ntnu.no

Abstract

When using support materials in heterogeneous catalysis, a fundamental understanding of the interactions between the catalyst and the support material is of critical importance. In this work, the stability, electronic structure, and catalytic activity of single-atom Pt catalysts on oxidized carbon support materials are investigated using first-principles calculations. The results are discussed based on both frontier-orbital hybridization and on a charge-transfer scheme. It is found that the strengthening of the Pt/C interactions by the carbon support with different oxygen concentrations is more due to charge transfer than frontier-orbital hybridization. In general, the larger the concentration of oxygen containg groups (OCGs) is and the closer they are to the Pt adatom, the stronger is the Pt binding energy to the carbon support. The dependence of the CO adsorption energy and CO vibrational stretching frequency on the concentration and the proximity of the OCGs to the Pt adatoms enables us to gauge quantitatively the effects of surface functionalization on the stability and catalytic activity of Pt catalysts. The change in the chemisorption energy of the CO molecule to the Pt adatom is discussed based on the position of the Pt $d-$band center, where it is found that it is shifted toward lower energy by increasing the concentration of OCGs. This downshift suppresses the coupling between the Pt $d-$band and the CO $2\pi^*$ state, and consequently both the catalytic activity and the CO adsorption energy are reduced. Our results suggest that tailoring the carbon support by oxygen-containing groups could provide a route for improving the tolerance of Pt/C catalysts to CO poisoning.

1 Introduction

Platinum nanoparticles supported by carbon nanostructures are widely applicable as catalysts in many chemical processes and fuel cell technologies.[1–4] However, the main challenge for these catalysts is still their efficiency which is low on a per metal atom basis since only the surface atoms are available for catalysis. Downsizing the catalyst nanoparticles even to a single atom is highly desirable to maximize their catalytic activity and selectivity, as well as utilization efficiency, but is, however, challenging.[5–7] There has been a significant progress on the synthesis and characterization of single-atom catalysts on different support materials, such as graphene[5] and metal-oxides.[7–9] The first practical fabrication of a single-atom Pt catalyst supported by iron oxide nanocrystallites was reported by Qiao *et al.*[8] It was shown that a single-atom Pt catalyst exhibits very high activity and stability for both CO oxidation and preferential oxidation of CO in H_2. Using atomic layer deposition, Sun *et al.* fabricated single atoms and sub-nanometer clusters of Pt on a surface of graphene nanosheet support.[5] They showed that single-atom catalysts exhibit significantly improved catalytic activity compared to commercial Pt/C catalysts.

The carbon support is supposed to stabilize the metal nanoparticles and to determine their size and degree of catalyst dispersion. The combination of high surface-to-volume ratio,[10] high electrical conductivity[11] and thermal stability[12] makes graphene a promising candidate for many potential applications such as catalyst support in fuel cells.[13–16] Progress in experimental techniques has made it possible to study the properties of graphene-supported metal nanoparticles such as Pt, Pd and Au,[17–20] which may offer a new type of carbon-based metal nanocomposite for the next generation of catalysts.

Thus, much effort has been devoted towards the understanding of the characteristics of the metal/carbon interface in heterogeneous catalysis.[21–27] However, diffusion and potential aggregation of catalyst particles under realistic working conditions, which limits their avail-ability and activity, are still among the important challenges.[28] An approach to solve this issue, while keeping the advantage of the high surface-to-volume ratio for graphene, is using chemically modified graphene to control the size and degree of the catalyst dispersion as well as the stability of catalyst particles to promote catalytic performance. One way of tailoring the chemical properties of graphene is doping with other atoms like B,[29] N,[30,31] P,[32] and Si.[33] Recent experimental studies indicate that N-doped graphene has great potential as a high-performance catalyst support for fuel cell electrocatalysis.[34] Using density functional theory (DFT) calculations, the hydrogen storage capacity of graphene is demonstrated to be improved by doping with B atoms.[35]

Another way of modifying the chemical properties of graphene is introducing a carbon vacancy into a graphene sheet. It was found that single Pt,[36] Fe,[37] and Au[38] adatoms on graphene defects show high chemical activity towards CO oxidation. In fact, a real graphene sheet get many carbon vacancies and defects during the preparation procedure, which under ambient conditions are initially saturated by stable oxygen-containing groups (OCGs), such as epoxy (C-O-C) and carbonyl.[39] Therefore, it is highly desirable to investigate the effects of OCGs on graphene-based Pt catalysts (Pt/G), which has received a great deal of attention in recent years, and it has been argued that OCGs are both beneficial[40–42] and detrimental[43–45] to catalyst dispersion. While Zhu *et al.*[45] reported that an oxygen-enriched carbon-nanofiber surface exhibits poor dispersion of Pt particles and low specific activity for the methanol oxidation reaction, other experiments indicate that existence of OCGs in Pt/G sheets exhibit excellent electrocatalytic activity towards methanol oxidation, outperforming commercial Pt/C electrocatalysts.[41] The results are exciting, however some fundamental questions remain open including the ability to control the electronic structure and the activity of supported Pt particles by modifying the chemical surrounding of the metal particles. The band-gap dependence of supported metal particles, among other important issues such as

the effects of OCGs on the electronic properties and stability of the carbon surface are also of high interest.

The adsorption of the CO molecule on Pt catalysts has been extensively studied because of its importance in various type of industrial catalytic reactions.[46–48] Furthermore, CO poisoning of Pt catalysts are still a severe challenge in fuel cell technology.[49] Recently, we investigated the effects of carbon-support on the electronic structure and catalytic activity of the Pt single-atom and dimer catalyst for CO adsorption.[50] It was found that the presence of the carbon surface not only stabilizes the Pt adatoms, but also significantly change the catalytic activity for CO chemisorption. The carbon support, by modifying the electron density surrounding the Pt adatoms, significantly change the hybridization between the $5d$ orbitals of the Pt adatoms and the $2\pi^*$ state of the CO molecule.

It is the purpose of the current study to offer an answer to some of the aforementioned questions by presenting a detailed analysis of the electronic structure, stability and catalytic activity of the Pt catalyst supported by edge-functionalized polycyclic aromatic hydrocarbons (PAH). First, we systematically study the band-gap dependence of the PAH surface on the edge functionalization, discussing the possibility of tailoring their electronic properties. Then we discuss how this can affect the electronic structure, stability and catalytic activity of the supported Pt catalyst, which is followed by studying CO adsorption.

2 Computational details

All quantum chemical calculations have been performed using the ADF software package.[51,52] DFT has been employed for the structural relaxation and energy minimization using the S12g[53] functional, which includes Grimme's D3 dispersion correction[54] and its performance for spin states of transition metal complexes is well documented.[23,50,53,55] This functional is the successor of the SSB-D functional,[56,57] which has been reported in a previous work[21] to have a better performance for describing the Pt/C system, comparing to the PBE,[58] PW91,[59]

and B3LYP[60] functionals. A mixed Slater-type basis set (TZ2P/QZ4P), where the QZ4P basis[61] (core triple$-\zeta$, valence quadruple$-\zeta$, four sets of polarization functions) is used for describing the Pt atom, and the TZ2P basis set[61] (core double$-\zeta$, valence triple$-\zeta$, two sets of polarization functions) is used to describe the C, O and the H atoms. The $1s$ electrons are kept frozen for the C atoms to speed up the calculations without affecting the accuracy of the results. The scalar relativistic effects are taken into account at the all-electron level with the zero-order-regular approximation (ZORA) approach.[62–67] This approach, demonstrated to have a small basis set superposition error,[68] has been successfully used to describe the Pt/C system in our previous work.[50]

The calculations were carried out using a polycyclic aromatic hydrocarbon ($C_{54}H_{18}$, circumcoronene) as a representative example for modelling the graphene surface, which has been found to be a suitable model system.[23,50] Geometry optimizations have been carried out using the BFGS (Broyden-Fletcher-Goldfarb-Shanno) algorithm[69] with the convergence criteria of 10^{-3} au in energy and of 10^{-3} au/Angstrom for the gradients. All structures were fully relaxed during the geometry optimization and a frequency analysis has been carried out ensuring the absence of imaginary frequencies and confirming each structure as a minimum on the potential energy surface. A tighter threshold in energy (10^{-6} au) gradient (10^{-5} au/Angstrom) have been used for systems with small imaginary frequency, however, no dramatic effect on the final energy was found (less than 10^{-2} eV). The adsorption energy for the Pt adatom and dimer, $E_{ads,Pt}$, on the oxidized-PAH ($C_{54}H_{18-x}O_x$) surface is calculated as

$$E_{ads,Pt} = E_{Pt_n/C_{54}H_{18-x}O_x} - E_{C_{54}H_{18-x}O_x} - E_{Pt_n} \tag{1}$$

where $E_{Pt_n/C_{54}H_{18-x}O_x}$, $E_{C_{54}H_{18-x}O_x}$, and E_{Pt_n} are the electronic ground state energies of the $Pt_n/C_{54}H_{18-x}O_x$ complex, the $C_{54}H_{18-x}O_x$ surface, and Pt_n, respectively. The CO adsorption

energy, $E_{ads,CO}$, is calculated as

$$E_{ads,CO} = E_{CO-Pt_n/C_{54}H_{18-x}O_x} - E_{Pt_n/C_{54}H_{18-x}O_x} - E_{CO} \quad (2)$$

where $E_{CO-Pt_n/C_{54}H_{18-x}O_x}$ and E_{CO} are electronic ground state energies for the $CO-Pt_n/C_{54}H_{18-x}O_x$ complex and a gas phase CO molecule, respectively. A more negative value of the adsorption energies indicates a stronger binding. Unrestricted calculations are adopted, where the spin state is denoted by the multiplicity $(2S+1)$ and the degree of spin contamination is assessed by inspection of the expectation value of $< S^2 >$, which ideally should be S(S+1) and thereby 0.00 for a singlet state, 0.75 for a doublet state, etc.

Density of states analysis[70] was carried out to further investigate the impact of OCGs on the electronic structure of the $Pt_n/C_{54}H_{18-x}O_x$ complexes. The Hirshfeld charge analysis,[71,72] which appears to be reliable and not very sensitive to basis set effects,[51] has been used to assign partial charges to the Pt adatoms.

3 Results and Discussions

3.1 Edge-functionalized PAH

We start by discussing the effects of OCGs on the electronic properties and stability of the PAH molecule since the electronic structure and catalytic activity of the Pt catalysts are affected by the electronic properties of the PAH support.[22,50] Hence, we considered a set of different OCGs, including hydroxy ($-$OH), epoxy ($-$epO), carbonyl ($-$C=O), carboxyl ($-$COOH), aldehyde ($-$CHO), ketone ($-$COCH$_3$), and the pyran-type of doping ($-$pyO) (see Figure 1). The energy levels of the highest occupied molecular orbital (HOMO), the lowest unoccupied molecular orbital (LUMO) and the HOMO–LUMO energy gap (ϵ_{HLG}), as well as the relative ground state stability (δG) for the edge-functionalized PAHs are compared to those of the pristine PAH molecule in Table 1. To account for the relative stability of different edge-functionalized PAHs, the molar (per atom) Gibbs free energy of formation, δG, was calcu-
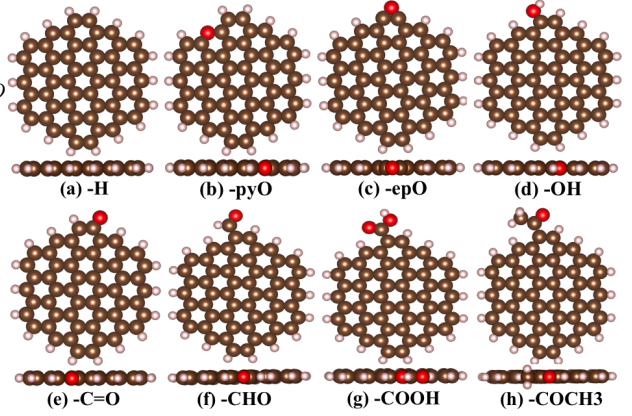

Figure 1: (a)−(h) Top and side views of relaxed structures of edge-functionalized PAHs. Carbon, oxygen, and hydrogen atoms are colored in brown, red and pink, respectively. The label below each graph indicates the functional group with which the PAH is functionalized.

Table 1: Relative stabilities, δG, HOMO energies, ϵ_H, LUMO energies, ϵ_L, and HOMO–LUMO energy gap, ϵ_{HLG}, of the PAHs with different functional groups, according to Figure 1. All energy terms are in eV.

structure	δG	ϵ_H	ϵ_{HLG}	ϵ_L
a	−0.087	−4.96	1.93	−3.03
b	−0.093	−3.81	0.22	−3.59
c	−0.041	−4.69	1.48	−3.21
d	−0.110	−4.88	1.88	−3.00
e	−0.098	−4.87	0.42	−4.45
f	−0.102	−5.13	1.37	−3.37
g	−0.130	−5.05	1.80	−3.25
h	−0.108	−5.08	1.85	−3.23

lated as[73]

$$\delta G = E_{coh} - \chi_C \mu_C - \chi_H \mu_H - \chi_O \mu_O \quad (3)$$

where χ_i is the molar fraction of atom i (i = C, O, H), and μ_i is the chemical potential of atom i at a given state. μ_H and μ_O are chosen as the binding energy per atom of the electronic ground state of the H$_2$ and O$_2$ molecules which are calculated to –2.29 and –3.45 eV, respectively. μ_C is given as the cohesive energy per atom of a single graphene sheet which is calculated to –7.99 eV. E_{coh} is the cohesive energy per atom of the system under consideration, which

is calculated as

$$E_{coh} = \frac{E_{system} - n_C E_C - n_H E_H - n_O E_O}{n_C + n_H + n_O} \quad (4)$$

where E_{system} is the total electronic energy of the model system, and n_C, n_H, n_O are the number of C, H, and O atoms, respectively. E_C, E_H, and E_O are the electronic energies of the corresponding free atoms in respective ground state, which are calculated to –1.23, –1.09, and –1.56 eV, respectively.

The usage of δG allows for a direct comparison between the stability of PAHs with a different stoichiometric composition. The largest negative δG value is found for the PAH functionalized by the carboxyl group followed by the hydroxy and other functional groups containing a carbon-oxygen double bond. This is consistent with thermal annealing at temperatures higher than $700\,^{\circ}\mathrm{C}$ for removing carboxyl and hydroxy groups from graphene oxides.[74]

As shown in Table 1, both the HOMO and LUMO energies of the PAHs functionalized with carboxyl, aldehyde, and ketone groups shift to lower energies as compared to pristine PAH. However, they shift to higher energies for the PAH functionalized with hydroxy group. For other functional groups, the energy of HOMO (LUMO) orbitals shift to higher (lower) energies. Li *et al.* proposed a mechanism based on a combination of frontier-orbital hybridization and charge transfer.[75] Frontier-orbital hybridization lowers ϵ_{HLG} via uneven shifts of the HOMO and LUMO, while charge transfer enlarges the energy gap through modification of the electronic screening. Therefore, the prominent down-shift of the LUMO of the PAHs functionalized with carbonyl and pyO groups is due to relatively large contributions of the orbitals of these functional groups to frontier-orbital hybridization. However, the impact of carboxyl, aldehyde, and ketone groups on the energy gap is much weaker, due to the cancellation of frontier-orbital hybridization effects by a large charge transfer. Thus, these functional groups together with the hydroxy group, although having relatively large impact on the stability of functionalized PAHs, they are not as effective in tuning the electronic properties. While the calculated absolute HLG values are sensitive to the choice of the XC functional, the trends of HLG for PAHs with different edge-functional groups are relatively comparable. These results presented here are in consistent with the results from edge-oxidized zigzag graphene nanoribbons (GNRs) using the screened exchange hybrid density functional HSE,[76] which has been shown to accurately reproduce experimental band gaps for a wide variety of materials.[77,78] They showed that the GNRs functionalized with carbonyl groups exhibits a vanishing band gap while other oxidized structures including hydrogenated, hydroxylated and lactonized GNRs have a band gap comparable to that of the fully hydrogenated ribbon, indicating that their electronic character is only slightly changed upon oxidation. Hence, we select edge carbonyl groups (ECGs) to study the effects of the oxidized PAH support on the electronic properties and catalytic activity of Pt catalysts.

We have in addition explored different concentrations of carbonyl groups, and found that PAHs with higher concentrations of oxygens give a higher relative stability (Figure 2). Moreover, ϵ_{HLG} decreases dramatically with increasing concentration of ECGs. However, for PAHs with large number of edge carbonyl groups ($x > 10$), ϵ_{HLG} increases slightly which may be due to the geometrical distortion occurring in the PAH plane.

ECG functionalization leads to a superior electrical conductivity and high thermal stability in the PAH surfaces which may give a possibility for controlling the chemical reactivity of the Pt catalysts according to[79]

$$\sigma \propto \exp \frac{-\epsilon_{HLG}}{2k_B T} \quad (5)$$

where σ is the electrical conductivity, k_B is Boltzmann's constant, and T is the temperature. From a catalytic perspective, systems with a smaller ϵ_{HLG} tend to be more reactive.[80,81] An important aspect of this study is therefore if an egde-functional group that change the electrical conductivity of a carbon substrate affects the electronic structure
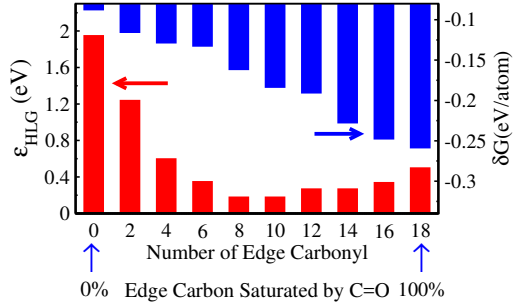
Figure 2: Correlation between δG and ϵ_{HLG} with the number of ECGs.

and chemical activity of a supported catalyst. Hence, in the next section we consider the effects of ECGs on the stability and catalytic activity of Pt catalysts supported by oxidized PAHs.

3.2 Pt Adsorption on Functionalized-PAH

Experiments indicate that the presence of active defect sites, such as OCGs, on Pt/G sheets will enhance the catalytic activity and tolerance to CO poisoning relative to commercial Pt/C catalysts.[41,42] In fact, the chemical surrounding of the Pt adatoms has a major effect on their catalytic activity. Hence, in this section we study the effects of oxidized PAHs on the adsorption properties, stability and electronic structure of the Pt catalyst.

We investigated adsorption properties of the Pt adatom and dimer on the bridge site of the surface, since the bridge site has been found to be the most favourable adsorption site for both the Pt adatom and dimer.[21,22] The results are shown in Table 2. Introducing carbonyl groups to the edge of the Pt_n/PAH complex (Figure 3), changes their electronic and structural properties. However, as for the $Pt/C_{54}H_{18}$ and $Pt_2/C_{54}H_{18}$ complexes, the spin ground state of the $Pt/C_{54}H_{18-x}O_x$ and $Pt_2/C_{54}H_{18-x}O_x$ ($x = 4, 8, 18$) complexes are singlet and triplet, respectively.

As the number of ECGs is increasing, the adsorption for both the Pt adatom and dimer becomes stronger (Table 2). The distance between the Pt adatom and the PAH surface (d_{Pt-C}) slightly decreases by increasing the number of
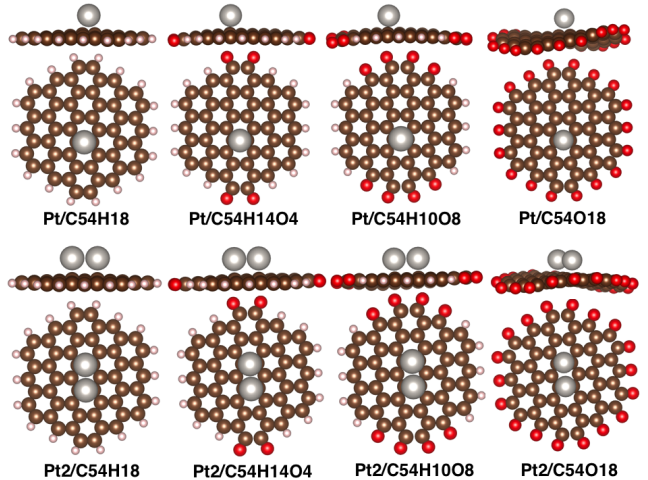

Figure 3: Top and side views of the $Pt_n/C_{54}H_{18-x}O_x$ complexes where $n = 1, 2$ and $x = 0, 4, 8,$ and 18. Gray, brown, red, and pink circles indicate Pt, C, O, and H atoms, respectively.

ECGs, indicating a stronger hybridization between the $5d$-orbitals of the Pt adatom and the 2π-orbitals of the carbon surface. The positive partial charges of the Pt adatom and dimer also increase, which is in line with a larger withdrawing of electrons from the π orbitals of the PAH surface by the ECGs (see Table 2). Indeed, there is a flow of electrons from the Pt adatoms to the oxygens through the carbon surface due to their electronegativity differences. Hence, both frontier-orbital hybridization and electrostatic effects play an important role in strengthening Pt/C interactions.

To further investigate the effect of ECGs on the electronic structure of the $Pt_2/C_{54}H_{18-x}O_x$ complexes, we analyzed the density of states obtained from spin–polarized DFT calculations. Although DOS calculations are sensitive to the choice of method, however DOS analysis is a popular method in surface science[82,83] and it can be used to qualitatively compare the effect of different ECGs. PDOS calculations are also sensitive to the basis set since they rely on a Mulliken-type of division of the orbitals, and Mulliken charges are known to be highly dependent on the basis set.[84,85] Figure 4 shows the total density of states (TDOS) of the $Pt_2/C_{54}H_{14}O_4$,

Table 2: Adsorption properties of the $Pt_n/C_{54}H_{18-x}O_x$ complexes in Figure 3.[a]

complex	2S+1	$E_{ads,Pt}$	d_{Pt-C}	Pt charge	O charge	complex	2S+1	E_{ads}	d_{Pt-C}	Pt charge	O charge
$Pt/C_{54}H_{18}$	1	−1.70	1.97	0.13	—	$Pt_2/C_{54}H_{18}$	1	−0.72	2.11, 2.12	0.07, 0.07	—
	3	−0.64	2.10	0.03	—		3	−0.82	2.07, 2.07	0.08, 0.08	—
$Pt/C_{54}H_{14}O_4$	1	−1.72	1.96	0.15	−0.77	$Pt_2/C_{54}H_{14}O_4$	1	−0.74	2.10, 2.11	0.10, 0.10	−0.77
	3	−0.91	1.98	0.13	−0.78		3	−0.82	2.07, 2.07	0.11, 0.10	−0.76
$Pt/C_{54}H_{10}O_8$	1	−2.00	1.96	0.17	−1.27	$Pt_2/C_{54}H_{10}O_8$	1	−1.35	2.05, 2.05	0.15, 0.15	−1.24
	3	−2.00	1.96	0.17	−1.27		3	−1.37	2.05, 2.05	0.15, 0.15	−1.24
$Pt/C_{54}O_{18}$	1	−1.94	1.94	0.18	−2.09	$Pt_2/C_{54}O_{18}$	1	−1.48	1.93, 1.92	0.21, 0.21	−2.09
	3	−1.68	1.95	0.19	−2.07		3	−1.49	1.93, 1.92	0.21, 0.21	−2.09

[a] The adsorption energy for Pt adatoms and dimers, $E_{ads,Pt}$, the height of the Pt adatom with respect to the averaged z coordinates of the C atoms (which are coordinated to the Pt adatom) in the PAH surface, d_{Pt-C}, the Hirshfeld atomic charge of Pt adatoms for different spin multiplicities (2S+1) of the corresponding complexes are given. O charge indicates the total number of electrons withdrawn from the Pt_n/PAH complex by edge oxygens. All energies are in eV, distances are in Å, and charges are in atomic units, $|e| = 1$.
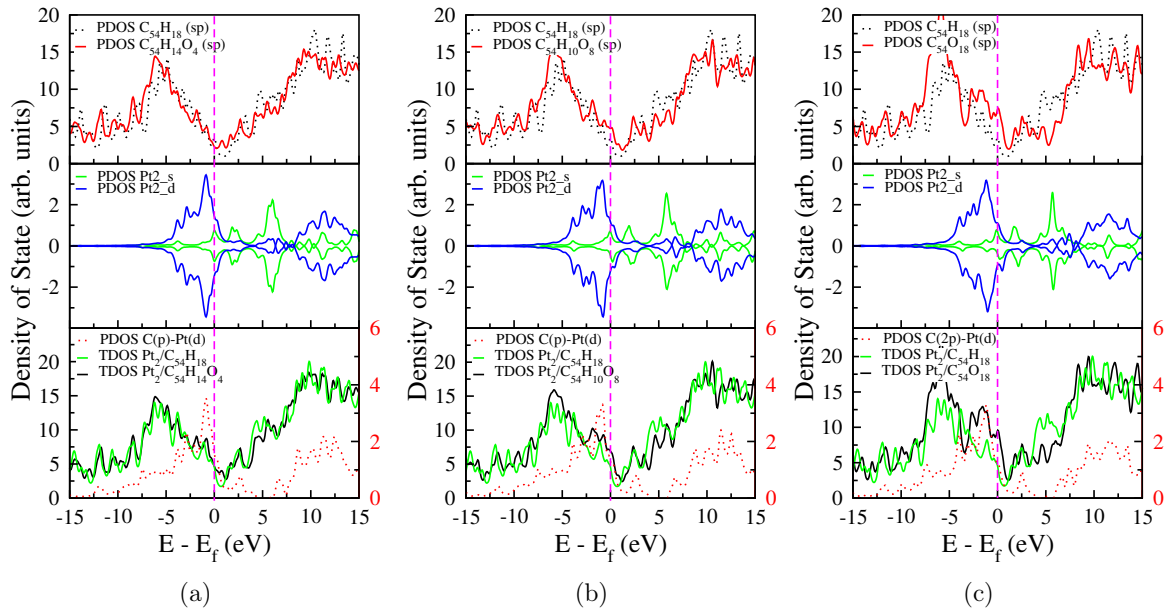

Figure 4: The TDOS of the $Pt_2/C_{54}H_{18-x}O_x$ complexes, as well as the density of states projected on the $C_{54}H_{18-x}O_x$ molecules are compared with that of the corresponding complexes before edge functionalization. The individual contribution from the Pt_s and the Pt_d, as well as the density of states projected on Pt_d and C_{2p} are also given. The a, b, and c plots correspond to the $Pt_2/C_{54}H_{18-x}O_x$ complexes where x is 4, 8, and 18, respectively. The vertical dashed line in each panel indicates the Fermi level which is shifted to 0 eV.

$Pt_2/C_{54}H_{10}O_8$, and the $Pt_2/C_{54}O_{18}$ complexes, as well as the partial contributions from the Pt_s and the Pt_d states. In each panel, the electronic structure of the $Pt_2/C_{54}H_{18-x}O_x$ complex and the $C_{54}H_{18-x}O_x$ molecule are compared to that of the corresponding complexes before edge functionalization, which indicates that the electronic structure of the PAH surface, as well as the adsorbed Pt dimer, are perturbed by edge functionalization. The energy levels shift to lower energy after introducing the ECGs. For example, the Fermi energy for the $Pt_2/C_{54}H_{14}O_4$, $Pt_2/C_{54}H_{10}O_8$, and the $Pt_2/C_{54}O_{18}$ complexes are calculated to −5.08, −5.54, and −6.33 eV, respectively.

An important finding from the DOS analysis is that by increasing the number of carbonyl groups, the intensity of the density of states projected on the C_{2p} and the Pt_{5d} states are slightly decreased (red dashed line in Figure 4),

indicating a reduction of hybridization between the Pt_{5d} and $C_{2\pi}$ states. Therefore, strengthening of the Pt/C interaction by increasing the ECGs is more due to electrostatic interactions rather than frontier-orbital hybridization. This is corroborated with the results from the Hirshfeld charge analysis where the partial charges on the Pt adatom increases with increasing number of ECGs (see Table 2).

3.3 CO adsorption

To investigate whether the catalytic properties of the Pt catalysts supported by an oxidized PAH surface differ from those of the PAH surface, we used the CO molecule as a probe molecule. The adsorption of the Pt adatom and dimer on the PAH surface is improved by ECGs, and although stability is a prerequisite for catalysts in practice,[86,87] changes in the electronic structure due to ECGs could also affect their catalytic activity.

In our previous work,[50,88] we studied different configurations for adsorption of the CO molecule on the atop and bridge sites of the Pt_2/PAH complex and the most stable configuration was found to be the configuration where the CO molecule is bonded to the bridge site of the Pt dimer, in agreement with previous studies.[89–92] In this configuration, both Pt atoms are in contact with the PAH surface and due to strong hybridization with the π orbitals of the PAH surface, both the Pt adatoms and the PAH surface can participate in electron transfer to the antibonding $2\pi^*$ orbital of the CO molecule. This bridge structure together with an atop structure for the Pt/PAH complex are our model systems to study the catalytic activity of Pt catalysts on oxidized PAH surfaces. It is worth noting that an asymmetric distribution of carbonyl groups to the edge of PAH surface causes moving of the CO–Pt complex toward the edge-carbonyl groups on the functionalized PAH surface, hence symmetrically doped structures were chosen (see Figure 5).

As for the Pt_n/PAH complex, introducing carbonyl groups to the edge of CO–Pt_n/PAH complex, changes their electronic and structural properties. However, the spin ground
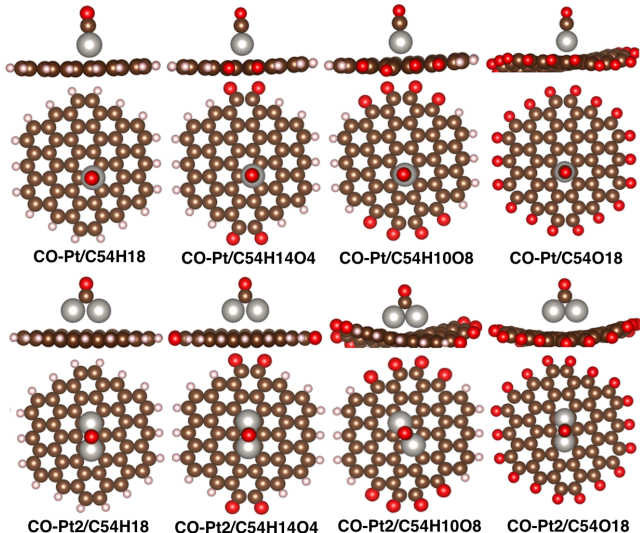

Figure 5: Top and side views of the CO−Pt_n/$C_{54}H_{18-x}O_x$ complexes where $n = 1$, 2 and $x = 1$, 2, 4, and 18. Gray, brown, red, and pink circles indicate Pt, C, O, and H atoms, respectively.

state of the CO–Pt/$C_{54}H_{18-x}O_x$ and CO–Pt_2/$C_{54}H_{18-x}O_x$ ($x = 4$, 8, 18) complexes remains singlet, as for the CO–Pt/$C_{54}H_{18}$ and CO–Pt_2/$C_{54}H_{18}$ complexes. The results are given in Table 3. The degree of spin contamination is checked by comparing the expectation value of $< S^2 >$ with the ideal value, S(S+1), which reflects in a small deviation ($< 10\%$) from the ideal value, except for systems with large structural deviations. For example, the degree of spin contamination for both the singlet and triplet states of the CO−Pt/$C_{54}H_{14}O_4$ complex is found to be zero, while the triplet state of the CO−Pt/$C_{54}O_{18}$ complex has the spin contamination of around 20%, however, its spin ground state (singlet state) has no contamination.

For both the Pt adatom and Pt dimer complexes, the Pt–C distance decreases and on the contrary, the Pt–C_{CO} distance increases slightly, as the number of ECGs is increasing. Therefore, the CO adsorption becomes weaker as compared to pristine PAH due to the presence of ECGs. The larger CO vibrational stretching frequency, ν_{CO}, as well as the shorter C−O bond length in the CO molecule as compared to pristine PAH also confirm the weakening of the Pt−CO interaction due to presence

Table 3: Results for adsorption of the CO molecule on the $Pt_n/C_{54}H_{18-x}O_x$ complexes with configurations according to Figure 5.[a]

		CO−Pt/$C_{54}H_{18-x}O_x$								CO−Pt$_2$/$C_{54}H_{18-x}O_x$					
x	2S+1	$E_{ads,CO}$	ν_{CO}	d_{Pt-C}	$d_{Pt-C_{CO}}$	d_{C-O}	Pt Charge	x	2S+1	$E_{ads,CO}$	ν_{CO}	d_{Pt-C}	$d_{Pt-C_{CO}}$	d_{C-O}	Pt Charge
0	1	−3.21	2037.9	2.24	1.79	1.159	0.06	0	1	−3.01	1825.3	2.91, 2.94	1.90	1.188	0.12, 0.12
	3	−1.41	2041.9	2.30	1.80	1.157	0.08		3	−2.24	1833.3	2.94, 2.96	1.90	1.187	0.12, 0.11
4	1	−3.00	2047.1	2.20	1.80	1.157	0.07	4	1	−2.95	1835.0	2.94, 2.96	1.91	1.186	0.12, 0.12
	3	−2.01	2050.6	2.21	1.81	1.155	0.10		3	−1.95	1841.7	2.94, 2.96	1.91	1.186	0.12, 0.12
8	1	−2.95	2056.0	2.17	1.81	1.154	0.11	8	1	−2.89	1872.8	2.22, 2.23	1.96	1.177	0.21, 0.21
	3	−2.94	2056.2	2.17	1.81	1.154	0.12		3	−2.66	1858.1	2.50, 2.59	1.93	1.180	0.19, 0.19
18	1	−2.81	2065.5	2.17	1.81	1.152	0.08	18	1	−2.14	1877.8	2.71, 2.78	1.92	1.179	0.16, 0.16
	3	−2.57	2066.0	2.17	1.81	1.152	0.08		3	−2.04	1888.3	2.31, 2.40	1.95	1.175	0.23, 0.22

[a] The CO adsorption energy, $E_{ads,CO}$, the height of the Pt adatom with respect to the averaged z coordinates of the C atoms (which are coordinated to the Pt adatom) in the PAH molecule, d_{Pt-C}, the distance between Pt adatom and the C_{CO} atom, $d_{Pt-C_{CO}}$, the CO bond length, d_{C-O}, the harmonic vibrational stretching frequency of the adsorbed CO, ν_{CO}, and the Hirshfeld atomic charge of Pt adatoms for different spin multiplicities (2S+1) of the corresponding complexes are given. All energies are in eV, distances in Å, frequencies in cm^{-1}, and charges are in atomic units, $|e| = 1$.

of ECGs (see Table 3).

The correlation between the C–O stretching frequency and the CO adsorption energy versus the number of ECGs is given in Figure 6. As expected, the C–O stretching frequency increases as the adsorption becomes weaker. In fact, ECGs withdraw electrons from the π orbitals of the PAH surface and consequently suppress the donation of electrons from π orbitals of the PAH surface to the $5d$ orbitals of the Pt adatoms. Therefore, the back−donation of electrons from the Pt_{5d} orbitals to the CO $2\pi^*$ orbitals also decreases. This is consistent with the Blyholder model[93] where the main feature is the back−donation of electrons from the d states of a metal atom to the antibonding $2\pi^*$ orbitals of a CO molecule. Moreover, the Hirshfeld charge analysis shows that by increasing the number of the ECGs, the partial charges on the Pt adatom and dimers are increasing, indicating a larger electron transfer from the Pt atoms to the oxidized PAH surface (Table 3).

To gain a more detailed insight of the electronic structure that play a role in the adsorption properties of the CO molecule, we analyzed the density of states projected on the adsorbed CO molecule before and after oxidation, as well as on the s and d states of the Pt adatoms. We also compared the TDOS of the CO−Pt$_2$/$C_{54}H_{18-x}O_x$ complexes with that of the CO−Pt$_2$/$C_{54}H_{18}$ complex to illustrate the effects of ECGs on the electronic structure of
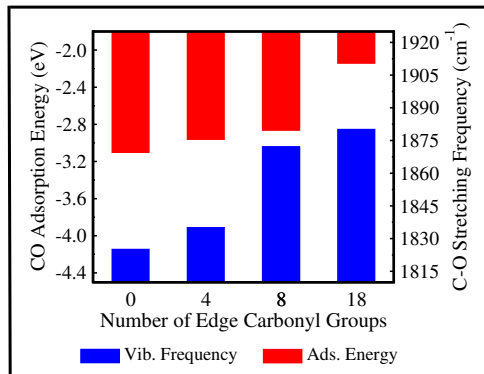

Figure 6: CO adsorption energy and C–O stretching frequency for the CO−Pt$_2$/$C_{54}H_{18-x}O_x$ are plotted versus the number of the ECGs.

these complexes. Hence, the differences in the density of states of theses complexes are due to the presence of ECGs (Figure 7). In all cases the $2\pi^*$ state of the adsorbed CO molecule is below the Fermi level, however, as the number of ECGs increases, the intensity of the CO $2\pi^*$ band is decreasing, which indicates that less electrons are transfered to the CO $2\pi^*$ state, comparing to the CO−Pt$_2$/$C_{54}H_{18}$ complex.

As shown in Figure 7, the ECGs have strong effects on the intensity and structure of the Pt d−bands. As the number of ECGs increases from 4 to 18, the sharpness and intensity of the Pt d−band decrease, and the contribution from the Pt_{5d} states to the frontier-orbitals of the corresponding complex is decreasing while
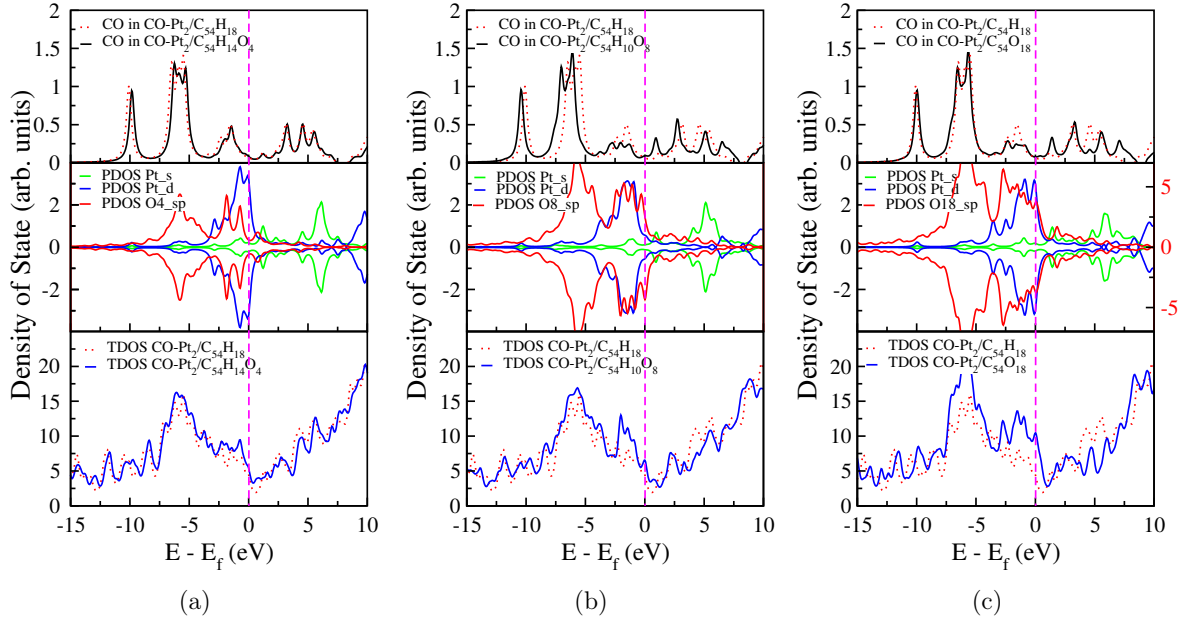
Figure 7: The total density of states of the $CO-Pt_2/C_{54}H_{18-x}O_x$ complexes, as well as the partial density of states projected on the adsorbed CO molecule, are compared with that on the $CO-Pt_2/C_{54}H_{18}$ complex. The individual contribution from the Pt_s, Pt_d and the O_{sp} states are also given. The a, b, and c plots correspond to the $CO-Pt_2/C_{54}H_{18-x}O_x$ complexes where x is 4, 8, and 18, respectively. The vertical pink dashed line in each panel indicates the Fermi level which is shifted to 0 eV.
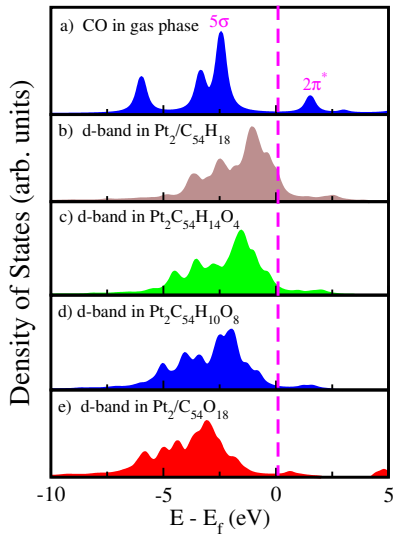

Figure 8: Density of states of (a) gas phase CO molecule, $d-$band of the Pt dimer supported by; (b) the PAH molecule, (c–e) the edge-oxidized PAHs. The energy levels of the Pt dâĽŠ-bands are relative to the Fermi level of the Pt_2/PAH complex which is shifted to zero.

the contributions from the sp states of the doped oxygens are increasing. This may sup-

press the hybridization between the Pt $d-$band and the CO $2\pi^*$ state (see Figure 7). Furthermore, the position of the $d-$band center is an important factor from a catalysis perspective, and could serve as an activity descriptor for transition metals.[94,95] A model for chemisorption on transition metals has been proposed, where the main feature is the importance of the position of the $d-$band center relative to the HOMO and LUMO of the adsorbate.[94,96] The change in the chemisorption energy of a CO molecule (δE_{chem}) due to a change in the position of the $d-$band center ($\delta\epsilon_d$) has been modeled as[97]

$$\delta E_{chem} \propto -4f_d \frac{V_{2\pi-d}^2}{(\epsilon_{2\pi} - \epsilon_d)^2}\delta\epsilon_d \qquad (6)$$

where f_d is the filling degree of the $d-$band, $V_{2\pi-d}$ is the coupling matrix element between the $d-$band and the $2\pi^*$ state, $\epsilon_{2\pi}$ is the energy of the $2\pi^*$ state, and ϵ_d is the position of the $d-$band center. Eq. 6 simplifies the interaction between the CO molecule and the Pt adatoms to a relation between an upwards (downwards)

shift of the $d-$band and an increased (decreased) stability of the CO molecule. Generally, the $d-$band center of a given metal atom depends on its surroundings, in which modifying the chemical surroundings of a transition metal by alloying,[98,99] overlayers[99] or by changing the coordination number of the metal atom,[100,101] could change its reactivity for a specific reaction.

The energy level of the Pt $d-$band, before and after oxidation, relative to the HOMO (5σ) and LUMO ($2\pi^*$) states of the gas phase CO molecule are shown in Figure 8. All energy levels of the Pt $d-$bands are relative to the Fermi level of the Pt_2/PAH complex to indicate the shift of the Pt $d-$band center after edge functionalization. As the number of ECGs increases, the position of the $d-$band is shifted toward lower energy to preserve the degree of $d-$band filling.[99] This downward shift suppresses the coupling between the Pt $d-$band and the CO $2\pi^*$ state. Hence, the farther the $d-$band center is from the Fermi level, the lower the CO adsorption energy. Therefore, it can be concluded that tailoring the carbon support through OCGs could provide a route for improving the tolerance of Pt/C catalysts against CO poisoning.

3.4 Pt–Doped–oxygen Distance

So far, we have considered the effects of the ECGs on adsorption and electronic structure of the Pt adatoms where although the ECG distance to the Pt adatoms is relatively large, 6–9 Å, their effect on the electronic structure of the Pt adatoms is considerable. It is therefore of interest to investiate how the proximity of the doped oxygens to the Pt adatom affects the catalytic properties. Hence, we systematically decrease the distance between the Pt adatom and a pyran-type doped oxygen in the PAH plane (Pt–O) and investigate the adsorption properties. The results are shown in Table 4. As the doped oxygen atom approaches the Pt adatom (Figure 9a–d), the Pt–C distance slightly decreases and the adsorption energy decreases, indicating a stronger interaction between the Pt adatom and the oxidized PAH sur-

face. ϵ_{HLG} increases by approaching the doped oxygen atom toward the Pt adatom which may suppress the activity of the Pt adatom in CO adsorption, in line with that ϵ_{HLG} is investigated as an indicator for measuring the electrical conductivity in eq. 5.

We also investigated the effect of the Pt–O distance on the adsorption of the CO molecule. The results are shown in Table 4. As the doped oxygen atom approaches the Pt adatom (Figure 9e–h), the Pt–C distance is decreasing, whereas the Pt—C_{CO} distance is increasing. Therefore, the CO adsorption becomes weaker, indicating a weaker interaction between the CO molecule and the Pt adatom. There is a correlation between the CO adsorption energy and ϵ_{HLG} of the $Pt/C_{53}H_{18}O$ complex, so that as the doped oxygen atom approaches the Pt adatom, the ϵ_{HLG} of the complex enlarges and consequently the CO adsorption becomes weaker. Moreover, the C–O stretching frequency also increases, indicating less back donation of electrons from the $5d$ orbitals of the Pt adatom to the $2\pi^*$ states of the adsorbed CO molecule. Therefore, it is also true that ϵ_{HLG} can be serve as an activity indicator for the single-atom Pt catalysts.
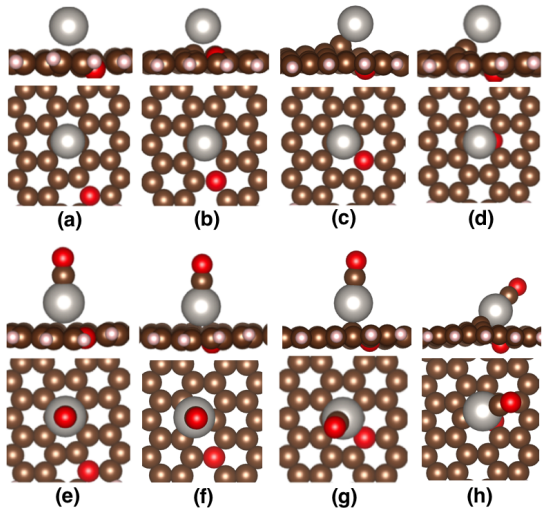

Figure 9: Top and side views of stable configurations for the $Pt/C_{53}H_{18}O$ complexes, before (a–d) and after (e–h) CO adsorption. The doped oxygen approches the Pt adatom from (a) $\rightarrow$ (d) and (e) $\rightarrow$ (h), respectively. Color coding is the same as in Figure 5.

Table 4: Results for adsorption properties of the Pt/C$_{53}$H$_{18}$O complex, before and after the CO adsorption, as a function of the Pt−O distance, according to Figure 9. The column headings are the same as in Table 3.

		before CO adsorption						after CO adsorption			
structure	2S+1	E$_{ads,Pt}$	ϵ_{HLG}	d$_{Pt-C}$	d$_{Pt-O}$	structure	2S+1	E$_{ads,CO}$	ν_{CO}	d$_{Pt-C}$	d$_{Pt-CO}$	d$_{C-O}$
a	1	−1.73	0.32	1.97	4.67	e	1	−3.03	2038.8	2.32	1.80	1.159
	3	−1.25	0.52	2.00	4.54		3	−2.39	2039.8	2.32	1.79	1.158
b	1	−1.96	0.66	1.94	3.38	f	1	−2.89	2045.9	2.24	1.79	1.157
	3	−1.49	0.27	1.95	3.31		3	−2.23	2049.2	2.23	1.80	1.157
c	1	−3.70	0.81	1.84	3.01	g	1	−1.54	2043.7	2.09	1.83	1.151
	3	−3.08	0.48	1.86	3.13		3	−1.53	2033.1	2.00	1.85	1.155
d	1	−3.82	0.83	1.83	3.08	h	1	−2.29	2053.1	2.04	1.88	1.151
	3	−3.05	0.35	1.87	3.12		3	−1.40	2035.8	2.00	1.86	1.155

4   Conclusions

DFT calculations have been used to characterize the influence of support functionalization on the catalytic performance of single-atom and dimer Pt catalysts. The stability, electronic structure, and catalytic activity of Pt catalysts supported by an O-functionalized carbon surface were discussed based on a combination of frontier-orbital hybridization and charge transfer. The stability of the Pt adatom increases by functionalizing the carbon support by OCGs, and depends the number and the proximity of the OCGs to the Pt adatoms. Using the Hirshfeld charge analysis, the vibrational stretching frequency of the CO molecule, and density of states analyses, it is found that the strengthening of the Pt/C interactions on the oxidized carbon support is more due to charge transfer than frontier-orbital hybridization.

The dependence of the CO adsorption energy and CO vibrational stretching frequency on the concentration and the proximity of the OCGs to the Pt adatoms were discussed based on the position of the Pt $d−$band center. It is found that the presence of OCGs in the carbon support leads to a downshift of the Pt $d−$band center and consequently weakens the binding strength of the CO molecule to the Pt catalyst. This is due to the suppressing of the coupling between the Pt $d−$band and the CO $2\pi^*$ state. Hence, the farther the $d−$band center is from the Fermi level, the lower is the CO adsorption energy. Our results demonstrate the usefulness of surface functionalization using OCGs to tailor the stability and catalytic efficiency of the Pt catalysts at the atomic scale and improve their tolerance to CO poisoning.

5   Acknowledgment

References

(1) Bell, A. The Impact of Nanoscience on Heterogeneous Catalysis. *Science* **2003**, *299*, 1688–1691.

(2) Wang, C.; Waje, M.; Wang, X.; Tang, J. M.; Haddon, R. C.; Yan, Y. S. Proton Exchange Membrane Fuel Cells with Carbon Nanotube Based Electrodes. *Nano Lett.* **2004**, *4*, 345–348.

(3) Thompson, S. D.; Jordan, L. R.; Forsyth, M. Platinum Electrodeposition for Polymer Electrolyte Membrane Fuel Cells. *Electrochim. Acta* **2001**, *46*, 657–1663.

(4) Basri, S.; Kamarudin, S.; Daud, W.; Yaakub, Z. Nanocatalyst for Direct Methanol Fuel Cell (DMFC). *Int. J. Hydrogen Energy* **2010**, *35*, 7957–7970.

(5) Sun, S.; Zhang, G.; Gauquelin, N.; Chen, N.; Zhou, J.; Yang, S.; Chen, W.; Meng, X.; Geng, D.; Banis, M. N. et al. Single-Atom Catalysis Using Pt/Graphene Achieved Through Atomic Layer Deposition. *Sci. Rep.* **2013**, *3*.

(6) Liang, S.; Hao, C.; Shi, Y. The Power of Single-Atom Catalysis. *ChemCatChem* **2015**, *7*, 2559–2567.

(7) Yang, X.-F.; Wang, A.; Qiao, B.; Li, J.; Liu, J.; Zhang, T. Single-Atom Catalysts: A New Frontier in Heterogeneous Catalysis. *Acc. Chem. Res.* **2013**, *46*, 1740–1748.

(8) Qiao, B.; Wang, A.; Yang, X.; Allard, L. F.; Jiang, Z.; Cui, Y.; Liu, J.; Li, J.; Zhang, T. Single-Atom Catalysis of CO Oxidation Using Pt_1/FeO_x. *Nat. Chem.* **2011**, *3*, 634–641.

(9) Moses-DeBusk, M.; Yoon, M.; Allard, L. F.; Mullins, D. R.; Wu, Z.; Yang, X.; Veith, G.; Stocks, G. M.; Narula, C. K. CO Oxidation on Supported Single Pt Atoms: Experimental and ab Initio Density Functional Studies of CO Interaction with Pt Atom on θ-Al_2O_3(010) Surface. *J. Am. Chem. Soc.* **2013**, *135*, 12634–12645.

(10) El-Kady, M. F.; Strong, V.; Dubin, S.; Kaner, R. Laser Scribing of High-Performance and Flexible Graphene-Based Electrochemical Capacitors. *Science* **2012**, *335*, 1326–1330.

(11) Proch, S.; Wirth, M.; White, H. S.; Anderson, S. L. Strong Effects of Cluster Size and Air Exposure on Oxygen Reduction and Carbon Oxidation Electrocatalysis by Size-Selected $Pt_n(n \leq 11)$ on Glassy Carbon Electrodes. *J. Am. Chem. Soc.* **2013**, *135*, 3073–3086.

(12) Wang, X.; Zhi, L.; Müllen, K. Transparent, Conductive Graphene Electrodes for Dye-Sensitized Solar Cells. *Nano Lett.* **2008**, *8*, 323–327.

(13) Scheuermann, G. M.; Rumi, L.; Steurer, P.; Bannwarth, W.; Mülhaupt, R. Palladium Nanoparticles on Graphite Oxide and Its Functionalized Graphene Derivatives as Highly Active Catalysts for the Suzuki-Miyaura Coupling Reaction. *J. Am. Chem. Soc.* **2009**, *131*, 8262–8270.

(14) Tang, L.; Wang, Y.; Li, Y.; Feng, H.; Lu, J.; Li, J. Preparation, Structure, and Electrochemical Properties of Reduced Graphene Sheet Films. *Adv. Funct. Mater.* **2009**, *19*, 2782–2789.

(15) Williams, G.; Seger, B.; Kamat, P. TiO2-Graphene Nanocomposites. UV-Assisted Photocatalytic Reduction of Graphene Oxide. *ACS Nano* **2008**, *2*, 1487–1491.

(16) Yoo, E.; Okada, T.; Akita, T.; Kohyama, M.; Honma, I.; Nakamura, J. Sub-nano-Pt Cluster Supported on Graphene Nanosheets for Co Tolerant Catalysts in Polymer Electrolyte Fuel Cells. *J. Power Sources* **2011**, *196*, 110–115.

(17) Yoo, E.; Okata, T.; Akita, T.; Kohyama, M.; Nakamura, J.; Honma, I. Enhanced Electrocatalytic Activity of Pt Subnanoclusters on Graphene Nanosheet Surface. *Nano Lett.* **2009**, *9*, 2255–2259.

(18) Gan, Y.; Sun, L.; Banhart, F. One- and Two-Dimensional Diffusion of Metal Atoms in Graphene. *Small* **2008**, *4*, 587–591.

(19) Xu, C.; Wang, X.; Zhu, J. Graphene-Metal Particle Nanocomposites. *J. Phys. Chem. C* **2008**, *112*, 19841–19845.

(20) Muszynski, R.; Seger, B.; Kamat, P. V. Decorating Graphene Sheets with Gold Nanoparticles. *J. Phys. Chem. C* **2008**, *112*, 5263–5266.

(21) Cheng, H.-Y.; Åstrand, P.-O.; Chen, D.; Zhu, Y.-A.; Zhou, X.-G.; Li, P. Adsorption of a Single Pt Atom on Polyaromatic Hydrocarbons from First-Principle Calculations. *Chem. Phys. Lett.* **2013**, *575*, 76–80.

(22) Mahmoodinia, M.; Ebadi, M.; Åstrand, P.-O.; Chen, D.; Cheng, H.-Y.; Zhu, Y.-A. Structural and Electronic Properties of the Pt_n-PAH Complex ($n = 1, 2$) from Density Functional Calculations. *Phys. Chem. Chem. Phys.* **2014**, *16*, 18586–18595.

(23) Mahmoodinia, M.; Åstrand, P.-O.; Chen, D. Chemical Bonding and Electronic Properties of the Co Adatom and Dimer Interacting with Polyaromatic Hydrocarbons. *J. Phys. Chem. C* **2015**, *119*, 24425–24438.

(24) Fampiou, I.; Ramasubramanian, A. Binding of Pt Nanostructures to Point Defects in Graphene: Adsorption, Morphology, and Electronic Structure. *J. Phys. Chem. C* **2012**, *116*, 6543–6555.

(25) Sanz-Navarro, C. F.; Åstrand, P.-O.; Chen, D.; Rønning, M.; van Duin, A. C. T.; Jacob, T.; Goddard, W. A. Molecular Dynamics Simulations of the Interactions between Platinum Clusters and Carbon Platelets. *J. Phys. Chem. A* **2008**, *112*, 1392–1402.

(26) Müller, U.; Sattler, K.; Xhie, J.; Venkateswaran, N.; Raina, G. Scanning Tunneling Microscopy of Single Platinum Atoms and Small Platinum Clusters on Highly Oriented Pyrolytic Graphite. *J. Vac. Sci. Technol. B* **1991**, *9*, 829–832.

(27) Wang, Q. J.; Che, J. G. Origins of Distinctly Different Behaviors of Pd and Pt Contacts on Graphene. *Phys. Rev. Lett.* **2009**, *103*.

13

(28) Uzun, A.; Ortalan, V.; Hao, Y.; Browning, N. D.; Gates, B. C. Nanoclusters of Gold on a High-Area Support: Almost Uniform Nanoclusters Imaged by Scanning Transmission Electron Microscopy. *ACS Nano* **2009**, *3*, 3691–3695.

(29) Acharya, C. K.; Sullivan, D. I.; Turner, C. H. Characterizing the Interaction of Pt and PtRu Clusters with Boron-Doped, Nitrogen-Doped, and Activated Carbon: Density Functional Theory Calculations and Parameterization. *J. Phys. Chem. C* **2008**, *112*, 13607–13622.

(30) Sheng, Z.-H.; Shao, L.; Chen, J.-J.; Bao, W.-J.; Wang, F.-B.; Xia, X.-H. Catalyst-Free Synthesis of Nitrogen-Doped Graphene via Thermal Annealing Graphite Oxide with Melamine and Its Excellent Electrocatalysis. *ACS Nano* **2011**, *6*, 4350–4358.

(31) Jeong, H. M.; Lee, J. W.; Shin, W. H.; Choi, Y. J.; Shin, H. J.; Kang, J. K.; Choi, J. W. Nitrogen-Doped Graphene for High-Performance Ultracapacitors and the Importance of Nitrogen-Doped Sites at Basal Planes. *Nano Lett.* **2011**, *11*, 2472–2477.

(32) Maciel, I. O.; Campos-Delgado, J.; Cruz-Silva, E.; Pimenta, M. A.; Sumpter, B. G.; Meunier, V.; López-Urías, F.; Muñoz-Sandoval, E.; Terrones, H.; Terrones, M. et al. Synthesis, Electronic Structure, and Raman Scattering of Phosphorus-Doped Single-Wall Carbon Nanotubes. *Nano Lett.* **2009**, *9*, 2267–2272.

(33) Campos-Delgado, J.; Maciel, I. O.; Cullen, D. A.; Smith, D. J.; Jorio, A.; Pimenta, M. A.; Terrones, H.; Terrones, M. Chemical Vapor Deposition Synthesis of N-, P-, and Si-Doped Single-Walled Carbon Nanotubes. *ACS Nano* **2010**, *4*, 1696–1702.

(34) Xiong, B.; Zhou, Y.; Zhao, Y.; Wang, J.; Chen, X.; O'Hayre, R.; Shao, Z. The Use of Nitrogen-doped Graphene Supporting Pt Nanoparticles as a Catalyst for Methanol Electrocatalytic Oxidation. *Carbon* **2013**, *52*, 181–192.

(35) Zhou, Y. G.; Zu, X. T.; Gao, F.; Nie, J. L.; Xiao, H. Y. Adsorption of Hydrogen on Boron-Doped Graphene: A First-Principles Prediction. *J. Appl. Phys.* **2009**, *105*.

(36) Tang, Y. N.; Yang, Z. X.; Dai, X. Q. A Theoretical Simulation on the Catalytic Oxidation of CO on Pt/Graphene. *Phys. Chem. Chem. Phys.* **2012**, *14*, 16566–16572.

(37) Li, Y. F.; Zhou, Z.; Yu, G. T.; Chen, W.; Chen, Z. F. CO Catalytic Oxidation on Iron-Embedded Graphene: Computational Quest for Low-Cost Nanocatalysts. *J. Phys. Chem. C* **2010**, *114*, 6250–6254.

(38) Mao, K.; Li, L.; Zhang, W.; Pei, Y.; Zeng, X. C.; Wu, X.; Yang, J. A Theoretical Study of Single-Atom Catalysis of CO Oxidation Using Au Embedded 2D h-BN Monolayer: A CO-Promoted O_2 Activation. *Sci. Rep.* **2014**, *4*.

(39) Carlsson, J. M.; Hanke, F.; Linic, S.; Scheffler, M. Two-Step Mechanism for Low-Temperature Oxidation of Vacancies in Graphene. *Phys. Rev. Lett.* **2009**, *102*.

(40) Guha, A.; Lu, W. J.; Zawodzinski, T. A.; Schiraldi, D. A. Surface-modified Carbons as Platinum Catalyst Support for PEM Fuel Cells. *Carbon* **2007**, *45*, 1506–1517.

(41) Sharma, S.; Ganguly, A.; Papakonstantinou, P.; Miao, X.; Li, M.; Hutchison, J. L.; Delichatsios, M.; Ukleja, S. Rapid Microwave Synthesis of CO Tolerant Reduced Graphene Oxide-Supported Platinum Electrocatalysts for Oxidation of Methanol. *J. Phys. Chem. C* **2010**, *114*, 19459–19466.

(42) Sebastián, D.; Calderón, J. C.; González-Expósito, J. A.; Pastor, E.; Martínez-Huerta, M. V.; Suelves, I.; Moliner, R.; Lázaro, M. J. Influence of Carbon Nanofiber Properties as Electrocatalyst Support on the Electrochemical Performance for PEM Fuel Cells. *Int. J. Hydrogen Energy* **2010**, *35*, 9934–9942.

(43) Calvillo, L.; Gangeri, M.; Perathoner, S.; Centi, G.; Moliner, R.; Lazaro, M. J. Effect of the Support Properties on the Preparation and Performance of Platinum Catalysts Supported on Carbon Nanofibers. *J. Power Sources* **2009**, *192*, 144–150.

(44) Zaragoza-Martín, F.; Sõpena-Escario, D.; Morallón, E.; de Lecea, C. S.-M. Pt/carbon Nanofibers Electrocatalysts for Fuel Cells: Effect of the Support Oxidizing Treatment. *J. Power Sources* **2007**, *171*, 302–309.

(45) Zhu, J.; Zhao, T. J.; Kvande, I.; Chen, D.; Zhou, X. G.; Yuan, W. K. Towards a Highly-efficient Fuel-cell Catalyst: Optimization of Pt Particle Size, Supports and Surface-Oxygen Group Concentration. *Phys. Chem. Chem. Phys.* **2013**, *15*, 3803–3813.

(46) Huang, Y.-W.; Lee, S.-L. The B3LYP and BMK Studies of CO Adsorption on Pt(111): An Insight Through the Chemical Bonding Analysis. *Chem. Phys. Lett.* **2012**, *530*, 64–70.

(47) Ogletree, D. F.; van Hove, M. A.; Somorjai, G. A. LEED Intensity Analysis of the Structures of Clean Pt(111) and of CO Adsorbed on Pt(111) in the C(4×2) Arrangement. *Surf. Sci.* **1986**, *173*, 351–365.

(48) Blackman, G.; Xu, M.-L.; Ogletree, D. F.; Van Hove, M. A.; Somorjai, G. A. Mix of Molecular Adsorption Sites Detected for Disordered CO on Pt(111) by Diffuse Low-Energy Electron Diffraction. *Phys. Rev. Lett.* **1988**, *61*, 2352–2355.

(49) Hogarth, M. P.; Ralph, T. R. Catalysis for Low Temperature Fuel Cells PART 111: Challenges for the Direct Methanol Fuel Cell. *Platinum Metals Rev.* **2002**, *46*, 146–164.

(50) Mahmoodinia, M.; Åstrand, P.-O.; Chen, D. Influence of Carbon-Support on Electronic Structure and Catalytic Activity of Pt Catalysts: Binding to the CO Molecule. *J. Phys. Chem. C* **2016**, *120*, 12452–12462.

(51) te Velde, G.; Bickelhaupt, F. M.; Baerends, E. J.; Guerra, C. F.; van Gisbergen, S. J. A.; Snijders, J. G.; Ziegler, T. Chemistry with ADF. *J. Comput. Chem.* **2001**, *22*, 931–967.

(52) Guerra, C. F.; Snijders, J. G.; te Velde, G.; Baerends, E. J. Towards an Order-N DFT Method. *Theor. Chem. Acc.* **1998**, *99*, 391–403.

(53) Swart, M. A New Family of Hybrid Density Functionals. *Chem. Phys. Lett.* **2013**, *580*, 166–171.

(54) Grimme, S. Density Functional Theory with London Dispersion Corrections. *WIREs Comput. Mol. Sci.* **2011**, *1*, 211–228.

(55) Gruden-Pavlović, M.; Stepanović, S.; Perić, M.; Güell, M.; Swart, M. A Density Functional Study of the Spin State Energetics of Polypyrazolylborato Complexes of First-Row Transition Metals. *Phys. Chem. Chem. Phys.* **2014**, *16*, 14514–14522.

(56) Swart, M.; Solà, M.; Bickelhaupt, F. M. Switching Between OPTX and PBE Exchange Functionals. *J. Comput. Meth. Sci. Eng.* **2009**, *9*, 69–77.

(57) Swart, M.; Solà, M.; Bickelhaupt, F. M. A New All-Round Density Functional Based on Spin States and S_N2 Barriers. *J. Chem. Phys.* **2009**, *131*.

(58) Perdew, J. P.; Burke, K.; Ernzerhof, M. Generalized Gradient Approximation Made Simple. *Phys. Rev. Lett.* **1996**, *77*, 3865–3868.

(59) Perdew, J. P.; Chevary, J. A.; Vosko, S. H.; Jackson, K. A.; Pederson, M. R.; Singh, D. J.; Fiolhais, C. Atoms, Molecules, Solids, and Surfaces: Applications of the Generalized Gradient Approximation for Exchange and Correlation. *Phys. Rev. B: Condens. Matter Mater. Phys.* **1992**, *46*, 6671–6687.

(60) Stephens, P. J.; Devlin, F. J.; Chabalowski, C. F.; Frisch, M. J. Ab Initio Calculation of Vibrational Absorption and Circular Dichroism Spectra Using Density Functional Force Fields. *J. Phys. Chem.* **1994**, *98*, 11623–11627.

(61) Lenthe, E. V.; Baerends, E. J. Optimized Slater-type Basis Sets for the Elements 1-118. *J. Comput. Chem.* **2003**, *24*, 1142–1156.

(62) Heully, J. L.; Lindgren, I.; Lindroth, E.; Lundqvist, S.; Martensson-Pendrill, A. M. Diagonalisation of the Dirac Hamiltonian as a Basis for a Relativistic Many-Body Procedure. *J. Phys. B: At. Mol. Phys.* **1986**, *19*, 2799–2815.

(63) van Lenthe, E.; Baerends, E. J.; Snijders, J. G. Relativistic Regular Two-Component Hamiltonians. *J. Chem. Phys.* **1993**, *99*, 4597–4610.

(64) van Lenthe, E.; Baerends, E. J.; Snijders, J. G. Relativistic Total Energy Using Regular Approximations. *J. Chem. Phys.* **1994**, *101*, 9783–9792.

(65) van Lenthe, E.; Snijders, J.; Baerends, E. The Zero-Order Regular Approximation for Relativistic Effects: The Effect of Spin-Orbit Coupling in Closed Shell Molecules. *J. Chem. Phys.* **1996**, *105*, 6505–6516.

(66) van Lenthe, E.; van Leeuwen, R.; Baerends, E. J.; Snijders, J. G. Relativistic Regular Two-Component Hamiltonians. *Int. J. Quantum Chem.* **1996**, *57*, 281–293.

(67) van Lenthe, E.; Ehlers, A.; Baerends, E. Geometry Optimization in the Zero Order Regular Approximation for Relativistic Effects. *J. Chem. Phys.* **1999**, *110*, 8943–8953.

(68) Boys, S. F.; Bernardi, F. The Calculation of Small Molecular Interactions by the Differences of Separate Total Energies. Some Procedures with Reduced Errors. *Mol. Phys.* **1970**, *19*, 553–566.

(69) Schlegel, H. B. *Ab-Initio Methods in Quantum Chemistry*; Wiley: New York, 1987; Vol. I.

(70) Kittel, C.; McFadden, P. *Introduction to Solid State Physics*, 8th ed.; Wiley: New York, 1976.

(71) Hirshfeld, F. L. Bonded-Atom Fragments for Describing Molecular Charge Densities. *Theor. Chim. Acta* **1977**, *44*, 129–138.

(72) Wiberg, K. B.; Rablen, P. R. Comparison of Atomic Charges Derived via Different Procedures. *J. Comput. Chem.* **1993**, *14*, 1504–1518.

(73) Barone, V.; Hod, O.; Scuseria, G. E. Electronic Structure and Stability of Semiconducting Graphene Nanoribbons. *Nano Lett.* **2006**, *6*, 2748–2754.

(74) Gao, X.; Jang, J.; Nagase, S. Hydrazine and Thermal Reduction of Graphene Oxide: Reaction Mechanisms, Product Structures, and Reaction Design. *J. Phys. Chem. C* **2010**, *114*, 832–842.

(75) Li, Y.; Shu, H.; Niu, X.; Wang, J. Electronic and Optical Properties of Edge-Functionalized Graphene Quantum Dots and the Underlying Mechanism. *J. Phys. Chem. C* **2015**, *119*, 24950–24957.

(76) Heyd, J.; Scuseria, G. E.; Ernzerhof, M. Hybrid Functionals Based on a Screened Coulomb Potential. *J. Chem. Phys.* **2003**, *118*, 8207–8215.

(77) Heyd, J.; Scuseria, G. E. Efficient Hybrid Density Functional Calculations in Solids: Assessment of the Heyd-Scuseria-Ernzerhof Screened Coulomb Hybrid Functional. *J. Chem. Phys.* **2004**, *121*, 1187–1192.

(78) Heyd, J.; Peralta, J. E.; Scuseria, G. E.; Martin, R. L. Energy Band Gaps and Lattice Parameters Evaluated with the Heyd-Scuseria-Ernzerhof Screened Hybrid Functional. *123* **2005**, *123*, 1–8.

(79) Sheng, L. *Semiconductor Physical Electronics*; Springer: Berlin, 2006.

(80) Zhou, Z.; Parr, R. G. Activation Hardness: New Index for Describing the Orientation of Electrophilic Aromatic Substitution. *J. Am. Chem. Soc.* **1990**, *112*, 5720–5724.

(81) Aihara, J.-I. Correlation Found Between the Homo-Lumo Energy Separation and the Chemical Reactivity at the Most Reactive Site for Isolated-Pentagon Isomers of Fullerenes. *Phys. Chem. Chem. Phys.* **2000**, *2*, 3121–3125.

(82) Goesten, M. G.; Hoffmann, R.; Bickelhaupt, F. M.; Hensen, E. J. M. Eight-coordinate Fluoride in a Silicate Double-four-ring. *Proc. Natl. Acad. Sci. U. S. A.* **2017**, *114*, 828–833.

(83) Raupach, M.; Tonner, R. A Periodic Energy Decomposition Analysis Method for the Investigation of Chemical Bonding in Extended Systems. *J. Chem. Phys.* **2015**, *142*, 1–14.

(84) Åstrand, P.-O.; Ruud, K.; Mikkelsen, K. V.; Helgaker, T. Atomic Charges of the Water Molecule and the Water Dimer. *J. Phys. Chem. A* **1998**, *102*, 7686–7691.

(85) Swart, M.; van Duijnen, P. T.; Snijders, J. G. A Charge Analysis Derived from an Atomic Multipole Expansion. *J. Comput. Chem.* **2001**, *22*, 79–88.

(86) Zhang, X.; Lu, Z.; Xu, G.; Wang, T.; Ma, D.; Yang, Z.; Yang, L. Single Pt Atom Stabilized on Nitrogen Doped Graphene: CO Oxidation Readily Occurs via the Tri−molecular Eley−Rideal Mechanism. *Phys. Chem. Chem. Phys.* **2015**, *17*, 20006–20013.

(87) Kvande, I.; Chen, D.; Zhao, T.-J.; Skoe, I. M.; Walmsley, J. C.; Rønning, M. Hydrogen Oxidation Catalyzed by Pt Supported on Carbon Nanofibers with Different Graphite Sheet Orientations. *Top. Catal.* **2009**, *52*, 664–674.

(88) Presented data for these configurations in Ref.[50] were for the hollow site with constrained optimization.

(89) Sadek, M. M.; Wang, L. Effect of Adsorption Site, Size, and Composition of Pt/Au Bimetallic Clusters on the CO Frequency: A Density Functional Theory Study. *J. Phys. Chem. A* **2006**, *110*, 14036–14042.

(90) Sebetci, A. Interaction of Carbon Monoxide with Bimetallic Co-Pt Clusters: A Density Functional Theory Study. *Comput. Mater. Sci.* **2012**, *58*, 77–86.

(91) Lazić, P.; Alaei, M.; Atodiresei, N.; Caciuc, V.; Brako, R.; Blügel, S. Density Functional Theory with Nonlocal Correlation: A Key to the Solution of the CO Adsorption Puzzle. *Phys. Rev. B: Condens. Matter Mater. Phys.* **2010**, *81*.

(92) Roszak, S.; Balasubramanian, K. A Theoretical Study of Bridged vs Atop Interactions of Pt2 with CO. *J. Chem. Phys.* **1995**, *103*, 1043–1049.

(93) Blyholder, G. Molecular Orbital View of Chemisorbed Carbon Monoxide. *J. Phys. Chem.* **1964**, *68*, 2772–2777.

(94) Hammer, B.; Nørskov, J. K. Theoretical Surface Science and Catalysis-Calculations and Concepts. *Adv. Catal.* **2000**, *45*, 71–129.

(95) Hammer, B.; Nørskov, J. K. Why Gold is the Noblest of all the Metals. *Nature* **1995**, *376*, 238–240.

(96) Nørskov, J. K. Chemisorption on Metal Surfaces. *Rep. Prog. Phys.* **1990**, *53*, 1253–1296.

(97) Hammer, B.; Morikawa, Y.; Nørskov, J. K. CO Chemisorption at Metal Surfaces and Overlayers. *Phys. Rev. Lett.* **1996**, *76*, 2141–2144.

(98) Besenbacher, F.; Chorkendorff, I.; Clausen, B. S.; Hammer, B.; Molenbroek, A. M.; Nørskov, J. K.; Stensgaard, I. Design of a Surface Alloy Catalyst for Steam Reforming. *Science* **1998**, *279*, 1913–1915.

(99) Ruban, A.; Hammer, B.; Stoltze, P.; Skriver, H. L.; Nørskov, J. K. Surface Electronic Structure and Reactivity of Transition and Noble Metals. *J. Mol. Catal. A: Chem.* **1997**, *115*, 421–429.

(100) Hammer, B.; Nielsen, O. H.; Nørskov, J. K. Structure Sensitivity in Adsorption: CO Interaction with Stepped and Reconstructed Pt Surfaces. *Catal. Lett.* **1997**, *46*, 31–35.

(101) Hammer, B.; Nørskov, J. K. Adsorbate Reorganization at Steps: NO on Pd(211). *Phys. Rev. Lett.* **1997**, *79*, 4441.

Graphical TOC Entry